from "Clinical Dosimetry Measurements in Radiotherapy", eds D.W.O. Rogers and J.E. Cygler
Medical Physics Publishing (Madison WI) 2009

Appendix A

Stopping-Power Ratios, Ratios of Mass-Energy Absorption Coefficients and CSDA Ranges of Electrons

D.W.O. Rogers, Ph.D.
Carleton Laboratory for Radiotherapy Physics
Carleton University, Ottawa, Ontario, Canada

1. Introduction

As discussed in chapter 3, in the limit that a detector is a photon detector (i.e., it is sensitive to photons in the environment and not electrons from the surrounding medium) and if there is both charged particle equilibrium and the photon fluence in the detector and the medium are the same, we have

$$D_{med} = D_{det} \left(\frac{\overline{\mu_{en}}}{\rho} \right)_{det}^{med} . \quad \text{(A.1)}$$

In the limit that a detector is only sensitive to the electrons from the medium, Spencer-Attix cavity theory tells us that:

$$D_{med} = D_{det} \left(\frac{\overline{L}}{\rho} \right)_{det}^{med} . \tag{A.2}$$

In practice, detectors are often sensitive to both the electrons and the photons from the environment and Burlin cavity theory (Attix 1986; Burlin 1966, 1968) tells us that (see section 7 in chapter 3):

$$\frac{D_{det}}{D_{med}} = d \left(\frac{\overline{L}}{\rho} \right)_{med}^{det} + (1-d) \left(\frac{\overline{\mu_{en}}}{\rho} \right)_{med}^{det} , \tag{A.3}$$

where d is the fraction of the dose coming from electrons generated in the medium. Note that the ratios of doses in equation (A.3) are the inverses of those in the equations (A.1) and (A.2). In the limit of $d = 1$ we have an electron detector and in the limit of $d = 0$ we have a pure photon detector. Since what we need in practice is a correction by which we multiply the measured dose to the detector, a better way to write the equation is:

$$\frac{D_{med}}{D_{det}} = f(Q) = \frac{1}{\left(d \left(\frac{\overline{L}}{\rho} \right)_{med}^{det} + (1-d) \left(\frac{\overline{\mu_{en}}}{\rho} \right)_{med}^{det} \right)} . \tag{A.4}$$

While these specific formulae are of little numerical value in this day of Monte Carlo simulations of detectors, they do give a qualitative understanding of what is going on and in some cases present limiting values. If, for example, the ratio of mass-energy absorption coefficients and stopping-power ratios are both constant with particle energy and numerically close to each other, it is highly likely that the full Monte Carlo calculation will give an answer close to those ratios. If the values of these ratios change strongly with particle energy, then there is very likely a strong absorbed dose energy dependence, $f(Q)$. If the ratios differ considerably, and even if not, the details of the Monte Carlo calculation can be important. For example, Monte Carlo calculations are essential to take into account photon attenuation in a thick detector such as a TLD in low-energy x-rays or backscatter from the surroundings in a diode detector in an electron beam.

The purpose of this appendix is to present ratios of mass-energy absorption coefficients and stopping-power ratios as a function of particle energy for water to detection medium for a variety of commonly used materials. In addition, for those detectors used free-in-air, values of the ratio of mass energy absorption coefficients for air to detector medium are also given. The stopping-power ratios are for monoenergetic electron energies and in practice one needs the spectrum-averaged values (see chapter 3), so the values are given here only to indicate the expected range of the value.

In addition, there are some graphs of electron ranges in various materials as a function of energy and values of $\overline{g}$ for various materials as a function of energy.

2. Sources of the Data

The stopping-power ratios and mass-energy absorption coefficients are calculated using the EGSnrc system of codes (Kawrakow and Rogers 2000; Kawrakow 2000) where use is made of the XCOM dataset for photon cross sections (Berger and Hubbell 1987). The stopping power ratios utilize the ICRU Report 37 values of the mean ionization energy and density effect corrections when available (ICRU 1984; Berger 1992). If the ICRU density effect values are not available the default EGSnrc methods are used to calculate the mean ionization energy and density effect corrections for both the medium involved and water to provide more internal consistency. The restricted stopping powers are calculated by the EGSnrc code PEGS4 with a value of Δ = 10 keV.

The mass-energy absorption coefficients are calculated for an arbitrary material using the EGSnrc user-code *g* and the ratios taken to a data set for water. The values for water agree with the NIST data (Seltzer 1993) to better than 0.1%, as do the ratios of the values when available for comparison.

Compositions of all materials are summarized in table A-1. The compositions for radiochromic films and gel dosimeters were made available by Chris Soares (chapter 23) and John Schreiner and Tim Olding (chapter 30), respectively.

CSDA ranges of electrons are based on values in ICRU Report 37 as calculated using NIST's ESTAR programs (Berger 1992) as received by the author from Steve Seltzer.

Table A-1. Composition of Materials Reported on in this Appendix. The second column, labeled ICRU, specifies whether ICRU Report 37 values of the composition, I-value, and density effect were used (ICRU 1984). The last column gives the fraction by weight of each element of any consequence.

Material	ICRU	ρ (g/cm^3)	Composition
water	y	0.998	H:0.1119, O:0.8881
radiographic film			
Kodak	y	2.2	H:0.031, C:0.211, N:0.072, O:0.163, Br:0.223, Ag:0.301
nuclear	y	3.82	H:0.014, C:0.072, N:0.019, O:0.066, Br:0.349, Ag:0.474 S:0.0019, I:0.0031
LiF	y	2.635	Li:0.2676, F:0.7324
radiochromic film			
film			
GAF	n	1.08	H:0.093, C:0.566, N:0.157, O: 0.184
XRQA	n	1.20	H:0.064, C:0.381, N: 0.055, O:0.138, Li:0.040, Br:0.134 Cs: 0.223
EBT	n	1.10	H:0.094, C:0.574, N:0.132, O:0.164, Li:0.080, Cl:0.029
RTQA	n	1.10	H:0.091, C:0.537, N:0.127, O:0.142, Li:0.019, Cl:0.084
XR-T	n	1.20	H:0.078, C:0.462, N:0.115, O:0.143, Br:0.076, Cs:0.126
air	y	1.205E-3	C:1.24E-4, N:0.7553, O:0.2318, Ar:0.0128
OSL/Al_2O_3	y	3.97	O:0.471, Al:0.529
Si	y	2.33	Si:1.000
alanine	y	1.424	H:0.079, C:0.404, N:0.157, O:0.359
diamond	y	3.52	C:!.000
Fricke solution	y	1.024	H:0.108, O:0.880, Na:2.2E-5, S:0.013, Cl:3.5E-5, Fe: 5.5E-5
plastic scintillators			
scintillator	y	1.032	H:0.085, C:0.9
polystyrene	y	1.06	H:0.0774, C:0.923
gel dosimeters			
PAGAT	n	1.000[a]	H:0.107, C: 0.053, N:0.019, O:0.820, P:1.5E-4, S:1.1E-4,Cl:1.8E-4
Fricke-I[b]	n	1.005	H:0.109, C:0.021, N:0.0076, O:0.860, S:0.0018, Cl:4E-5, Na:2E-5,Fe:6E-5
Fricke-II[c]	n	1.005	H:0.1084, C:0.020, N:0.0067, O:0.858, S:0.0085, Cl:4E-5, Na:2.2E-5,Fe:2.6E-5
MAGIC	n	1.000*	H:0.105, C:0.084, N:0.012, O:0.797, Cu:1E-5,S:1.7E-4

[a] Density not known so unity used. Values of stopping-power ratios and mass-energy absorption coefficient ratios do not depend on the density.
[b] Schreiner and Olding, chapter 30
[c] Keall and Baldock (1999).

3. Ratios of Water to Detector Medium of Mass-Energy Absorption Coefficients and Stopping Powers

3.1 Air Ion Chambers

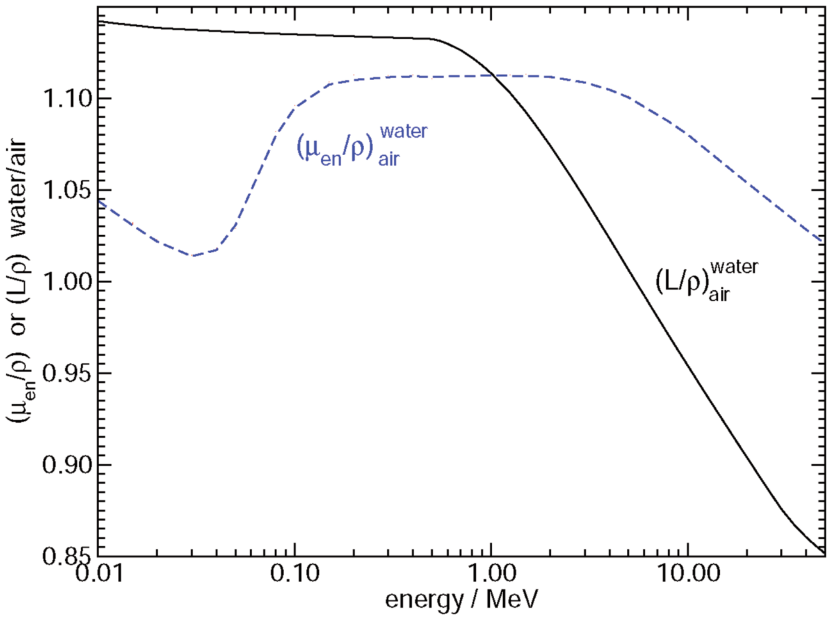

Figure A-1. Values of the ratios, water to air, of the restricted mass collision stopping powers, $\left(L_{\Delta}/\rho\right)_{air}^{water}$ with Δ = 10 keV and of mass energy absorption coefficients, $\left(\mu_{en}/\rho\right)_{air}^{water}$.

For ion chambers, only the stopping-power ratios are of any relevance since one never achieves CPE in the air so that the ratio of mass-energy absorption coefficients is not relevant for application of equation (A.1). However it may be used to estimate the ratio of air kerma to water kerma in a phantom when using a chamber calibrated in terms of air kerma (x-ray beams).

3.2 LiF TLDs

The stopping-power ratios for LiF are given for Δ = 10 keV, but in practice much higher values are needed. The unrestricted stopping-power ratios, which represent a limiting case for larger values of Δ, are 1 to 1.5% lower between 1 and 10 MeV.

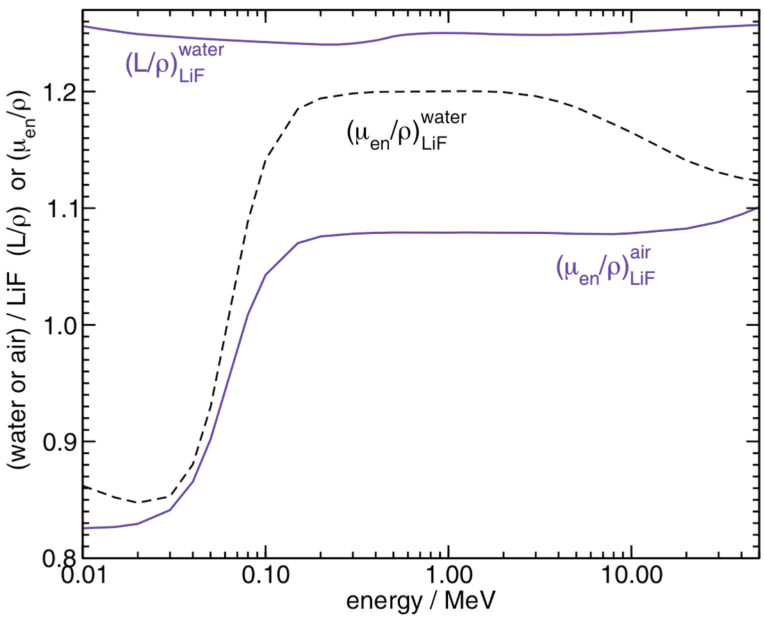

Figure A-2. Values of the ratios, water to LiF material, of the restricted mass collision stopping powers, $\left(L/\rho\right)^{water}_{LiF}$ for D = 10 keV and of the mass energy absorption coefficients, $\left(\mu_{en}/\rho\right)^{water}_{LiF}$. In addition, the data for LiF and air are given.

3.3 Radiochromic Films

Table A-1 gives the composition of five different materials that are or have been used as the sensitive components of GafChromic film (based on data in chapter 23). Figure A-3 presents the ratios above 100 keV and figure A-4 the values below 600 keV.

To the extent that these detectors are usually thought of as electron detectors, at least at higher energies, the variation of the stopping-power ratio suggests one would expect $f(Q)$ to vary by no more than 2% for "emulsion" (GAF) and EBT films and somewhat more for XRQA films.

For low-energy photons the situation is very complex because of the large variation of the ratio of mass-energy absorption coefficients and also the large difference between the stopping-power ratios and the ratios of mass-energy absorption coefficients. Full Monte Carlo calculations are required to establish the expected variation in $f(Q)$.

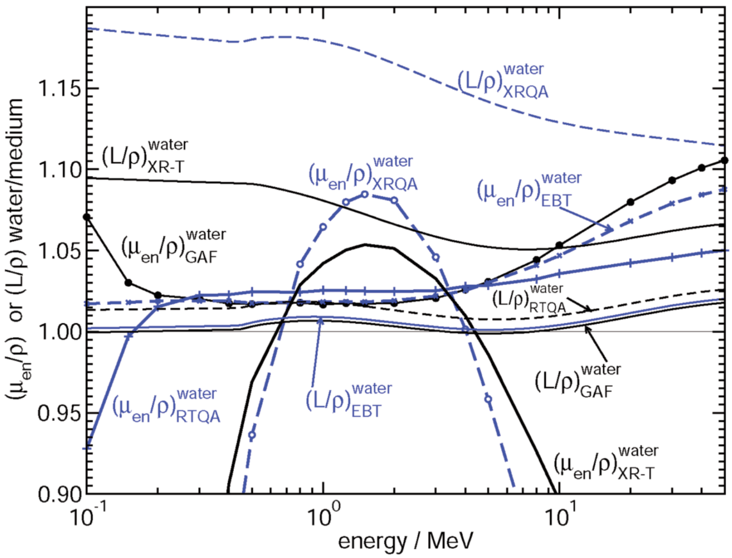

Figure A-3. Restricted mass collision stopping-power ratios and ratios of mass-energy absorption coefficients for the sensitive materials in radiochromic films relative to water. Compositions defined in table A-1.

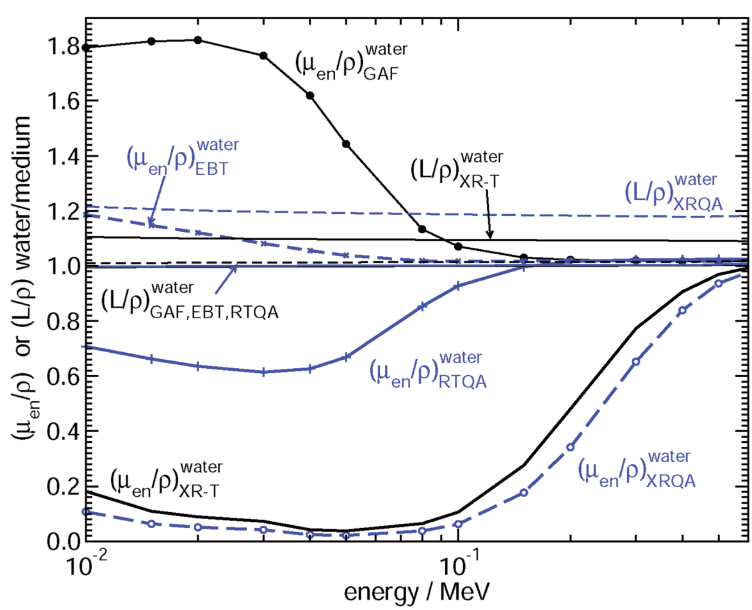

Figure A-4. As in figure A-3 but including lower energies.

3.4 Al_2O_3/OSL

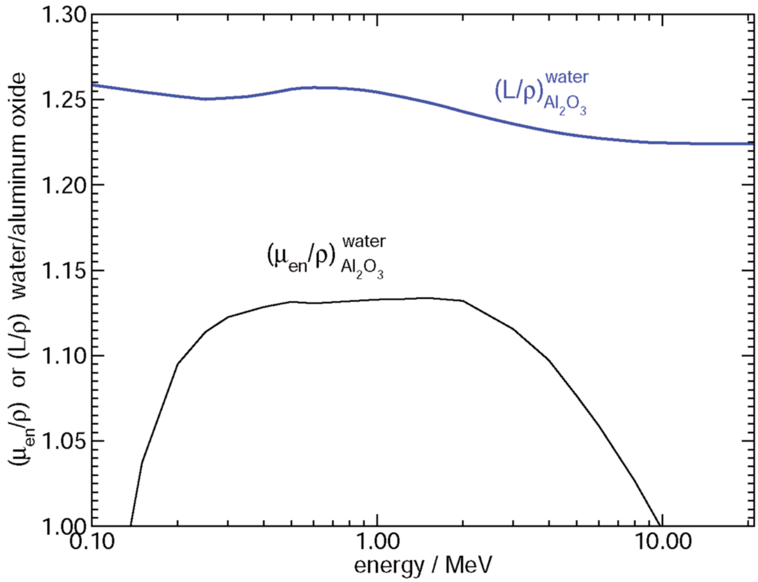

Figure A-5. Values for OSL detectors of the ratios, water to Al2O3, of the restricted mass collision stopping powers, $(L/\rho)^{water}_{Al_2O_3}$ and of the mass-energy absorption coefficients, $(\mu_{en}/\rho)^{water}_{Al_2O_3}$.

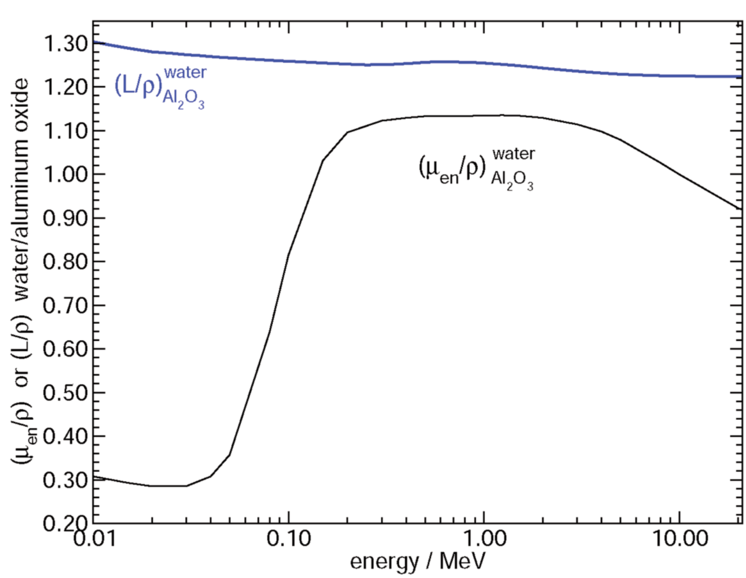

Figure A-6. Same as figure A-5 but including lower-energy range.

3.5 Silicon/MOSFETS, Diodes

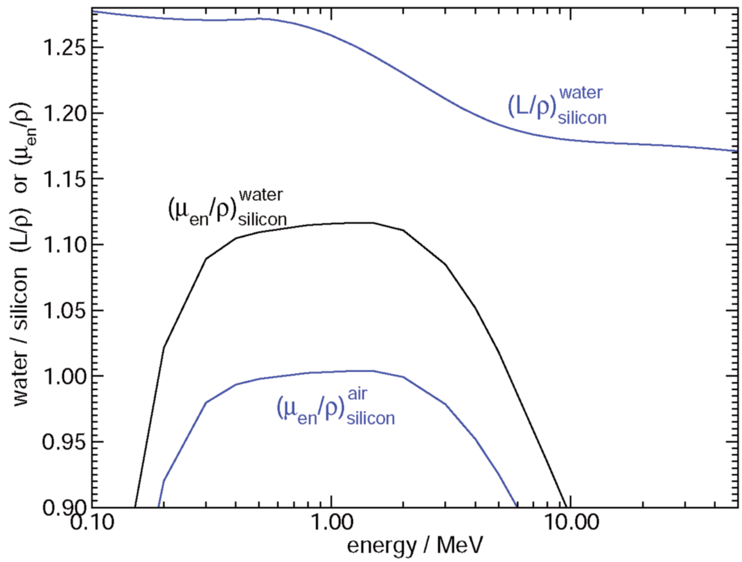

Figure A-7. Values of the ratios, water to silicon, of the restricted mass collision stopping powers, $\left(L/\rho\right)_{silicon}^{water}$ and the mass-energy absorption coefficients, $\left(\mu_{en}/\rho\right)_{silicon}^{water}$. In addition, the data for silicon and air are given.

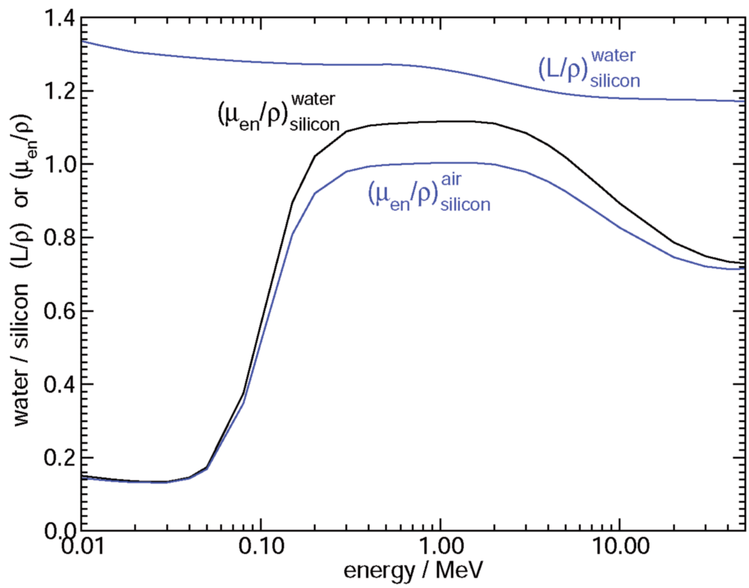

Figure A-8. As in figure A-7 but including the lower-energy range.

3.6 Alanine

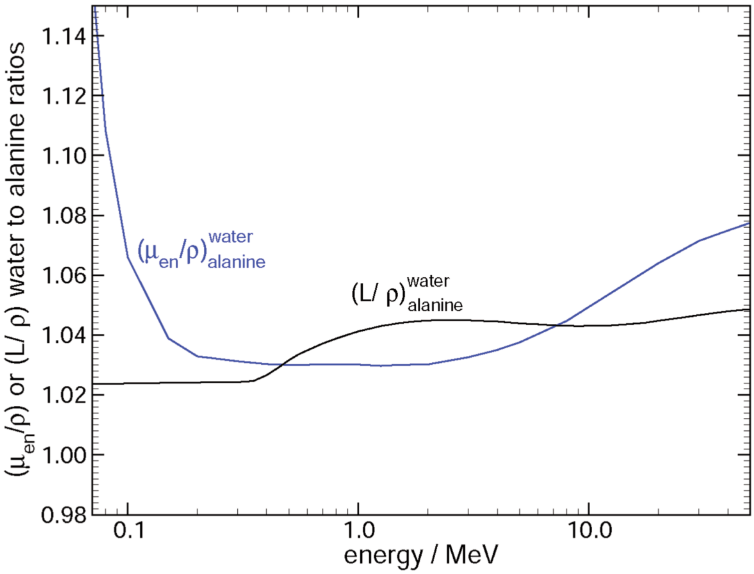

Figure A-9. Ratios of mass-energy absorption coefficients and electron restricted mass collision stopping powers for water to alanine. Actual alanine pellets have binders that can affect these values (Zeng et al. 2005).

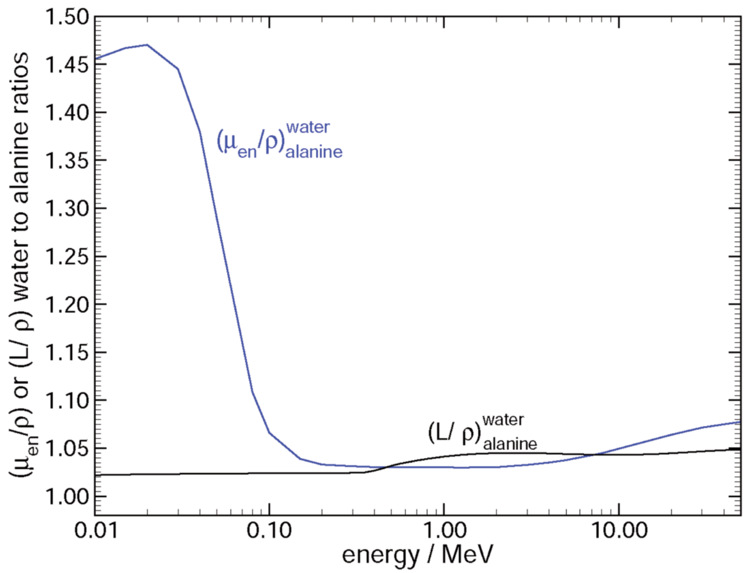

Figure A-10. As in figure A-9 but including low-energy range.

3.7 Diamond

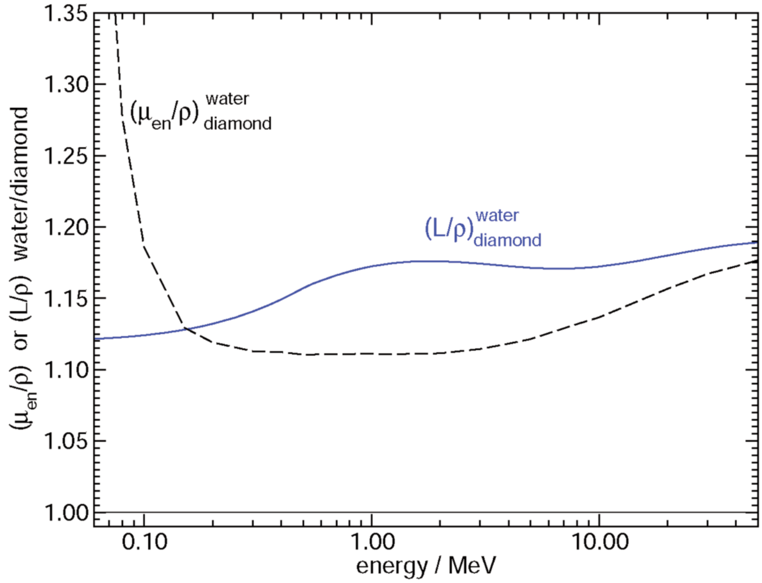

Figure A-11. Values of the ratios, water to diamond, of the restricted mass collision stopping powers, $(L/\rho)^{water}_{diamond}$ (Δ = 10 keV) and the mass-energy absorption coefficients, $(\mu_{en}/\rho)^{water}_{diamond}$. Density of diamond taken as $\rho = 3.52$ g/cm^2.

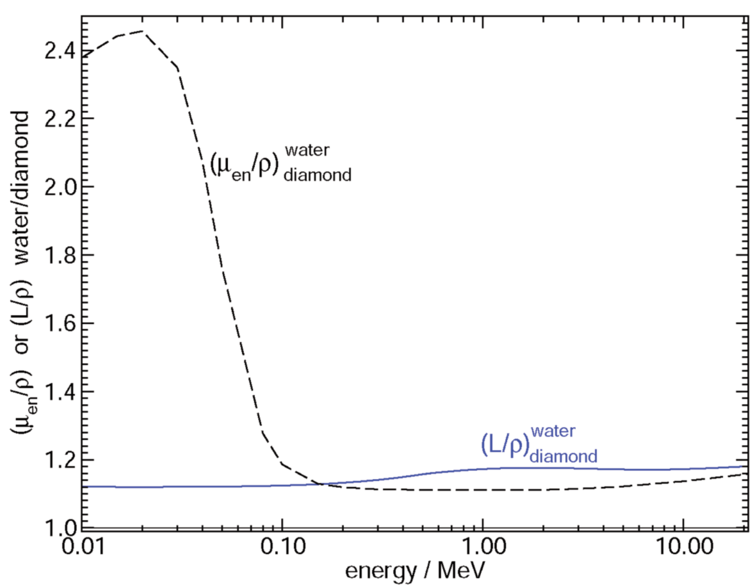

Figure A-12. As figure A-11 but including lower energies as well.

3.8 Fricke

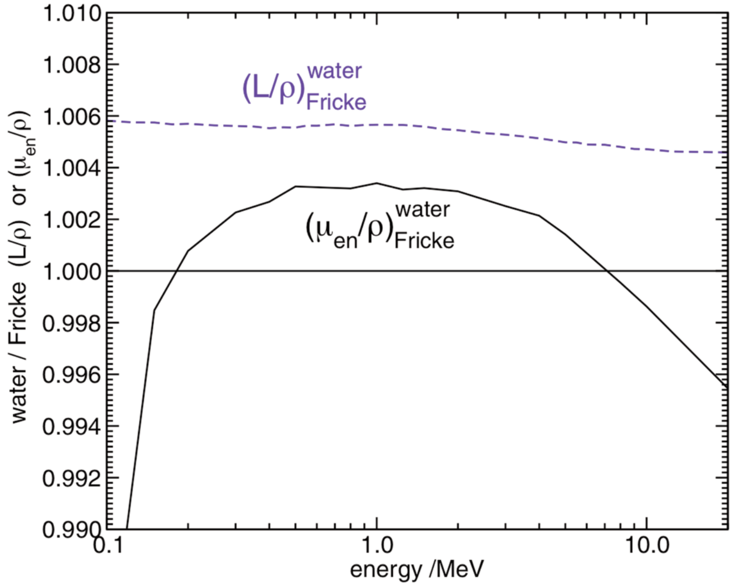

Figure A-13. Values of the ratios, water to Fricke solution, of the restricted mass collision stopping powers, $(L/\rho)^{water}_{Fricke}$ and of the mass-energy absorption coefficients, $(\mu_{en}/\rho)^{water}_{Fricke}$.

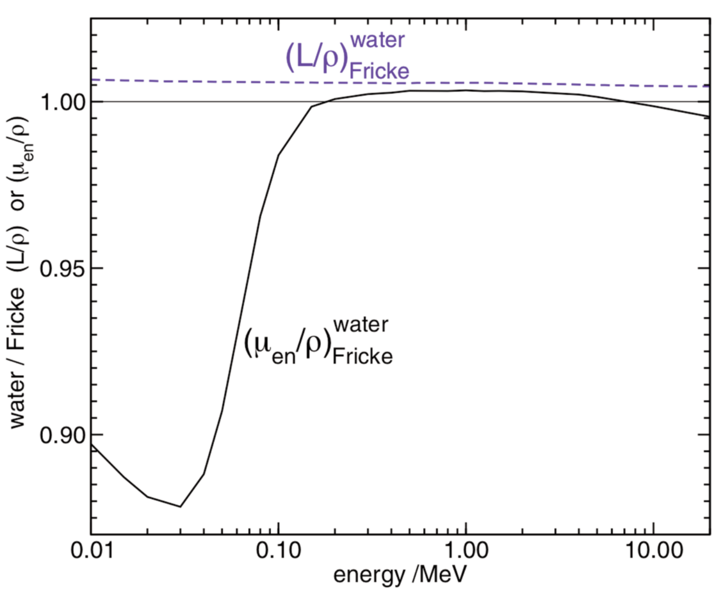

Figure A-14. As figure A-13 but including lower energies as well.

3.9 Plastic Scintillators

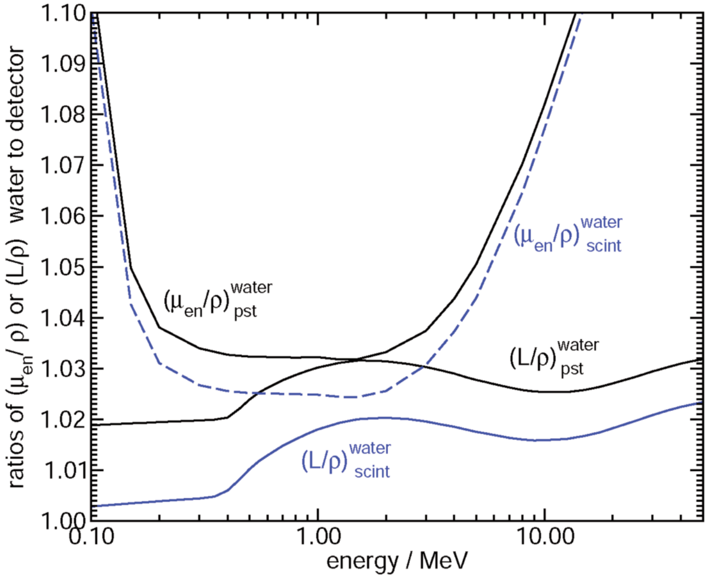

Figure A-15. Values of the ratios, water to two forms of plastic scintillator (polystyrene and ICRU Report 37 "plastic scintillator"), of the restricted mass collision stopping powers, $(L/\rho)^{water}_{detector}$ and of the mass-energy absorption coefficients, $(\mu_{en}/\rho)^{water}_{detector}$.

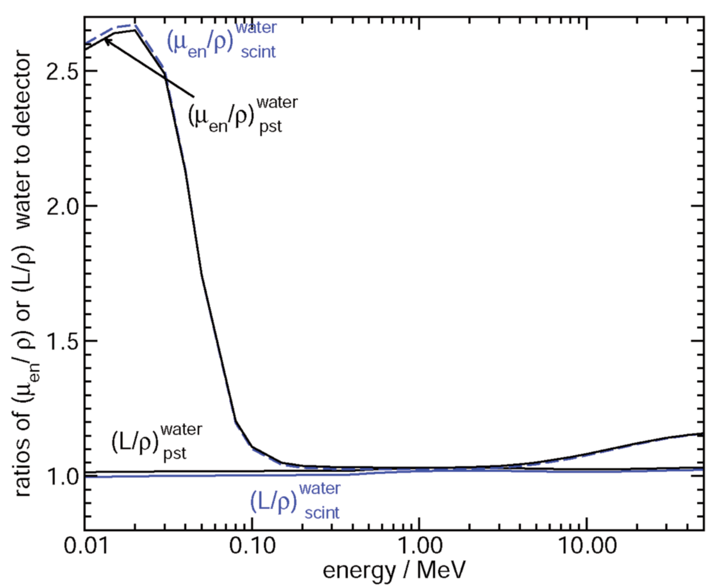

Figure A-16. Same as figure A-15 but including lower-energy range.

3.10 Radiographic Film

Due to the crystalline nature of the radiographic film, it is unclear if the standard data are meaningful in detail. Nonetheless they give an indication of the responses to be expected.

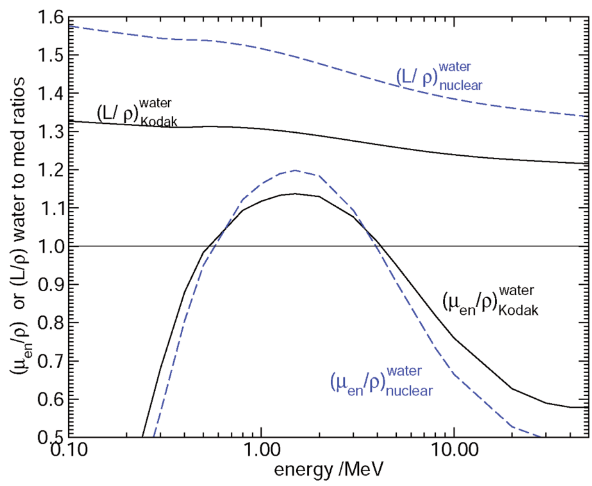

Figure A-17. Values of the ratios, water to two forms of radiographic film (a nuclear emulsion and Kodak aa&m film), of the restricted mass collision stopping powers, $(L/\rho)^{water}_{medium}$ and of the mass-energy absorption coefficients, $(\mu_{en}/\rho)^{water}_{medium}$.

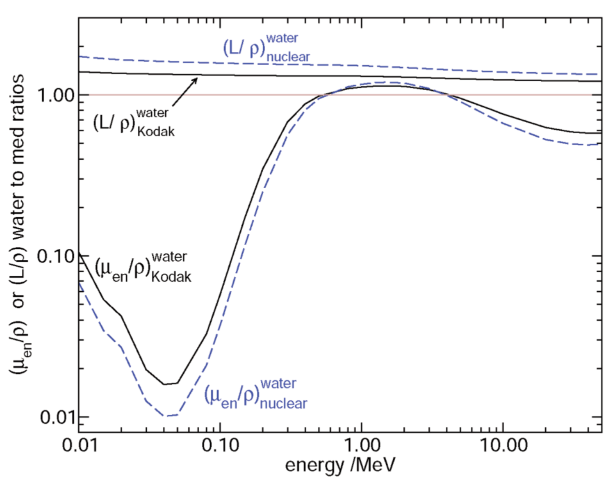

Figure A-18. Same as figure A-17 except including lower energies and with logarithmic y-axis.

3.11 Gel Dosimeters

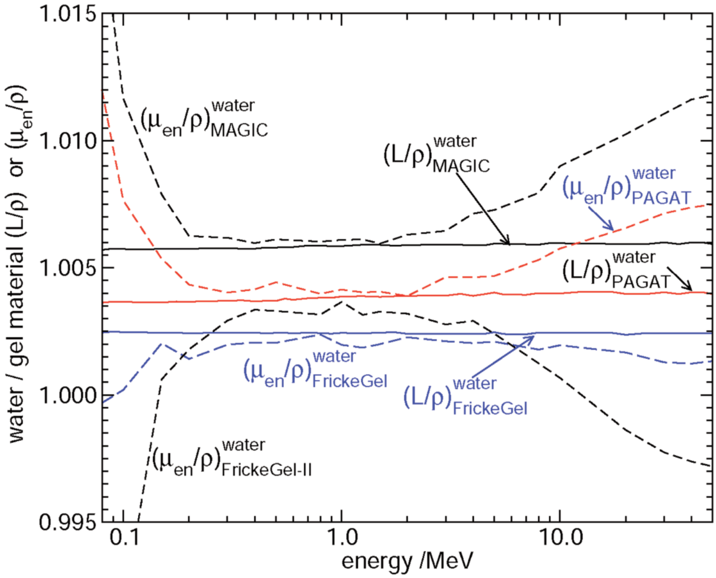

Figure A-19. Values of the ratios, water to three forms of gel dosimeters, of the restricted mass collision stopping powers, $(L/\rho)^{water}_{detector}$ and of the mass-energy absorption coefficients, $(\mu_{en}/\rho)^{water}_{detector}$.

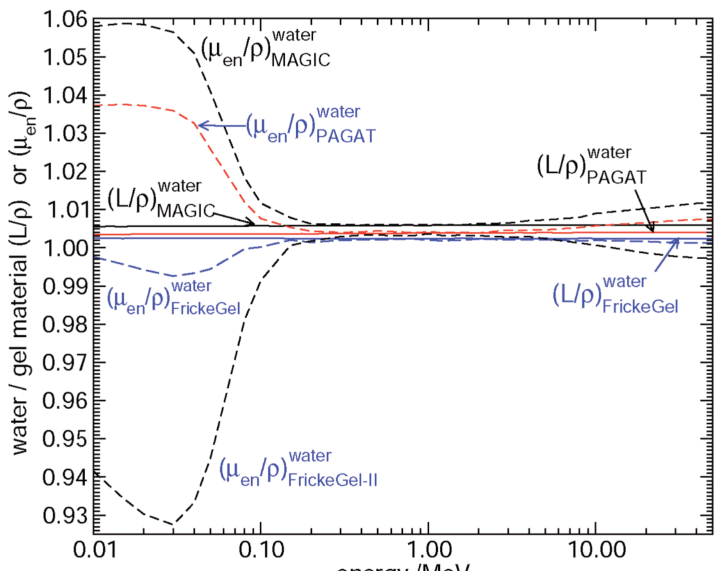

Figure A-20. Same as figure A-19 but including lower energy range.

4. CSDA Ranges of Electrons

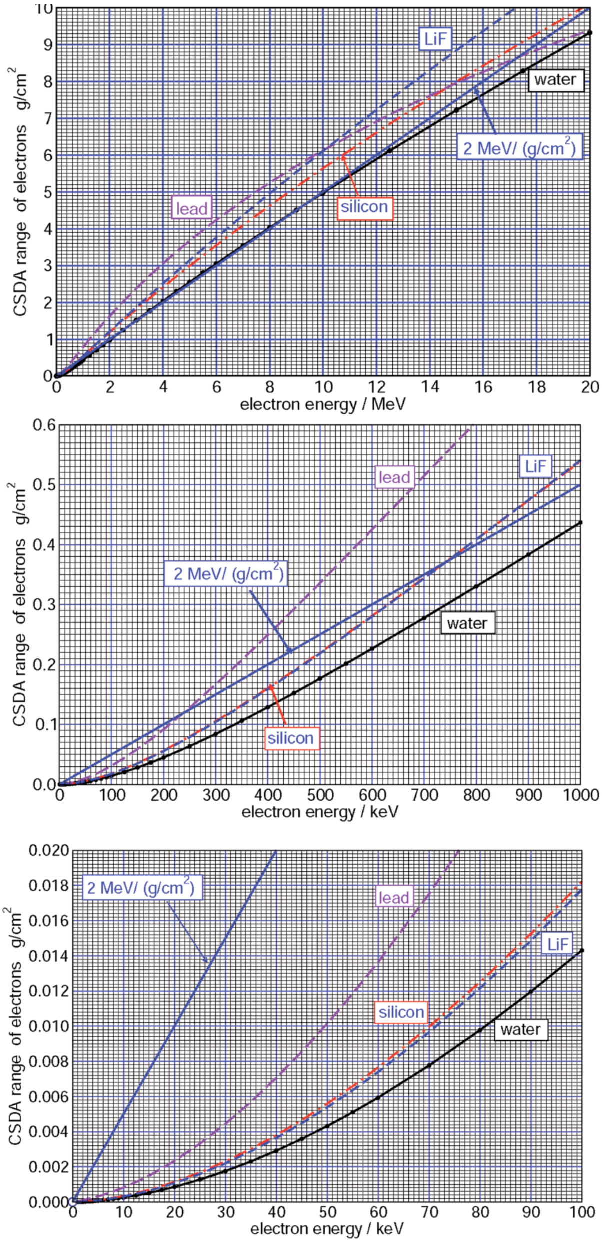

Figure A-21. CSDA ranges of electrons slowing down in the materials shown, based on calculations done by the author with ESTAR (Berger 1992). The range expected using the 2 MeV/(g/cm^2) rule of thumb is shown for comparison.

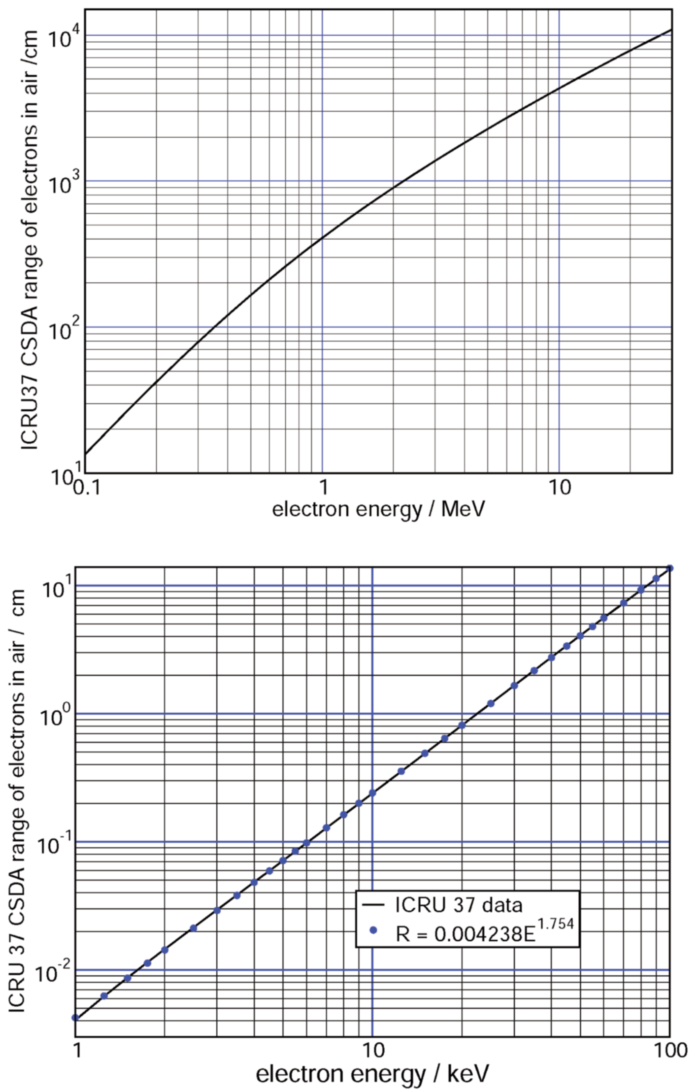

Figure A-22. CSDA ranges of electrons slowing down in air, based on calculations by the author with ESTAR (Berger 1992). The low-energy range (<100 keV) is fit within 1.5% for all energies except 1 keV by the expression $R = 0.004238E^{1.754}$ where the electron's kinetic energy is in keV and the range in cm.

5. g Values: Average Energy Lost to Radiative Events

The quantity $\overline{g}$ is the average fraction of the kinetic energy of secondary charged particles (produced in all the types of interactions) that is subsequently lost in radiative (photon-emitting) energy-loss processes as the particles slow to rest in the medium. The definitive paper on the subject is by Seltzer (1993).

Figures A-23 and A-24 present $\overline{g}$ values as a function of incident photon beam energy in a variety of materials. The values were calculated using the EGSnrc user-code "g" with the XCOM dataset. Note that the structure at low energies is related to the average energy of the electrons, which is much higher in photoelectric interactions than in Compton interactions.

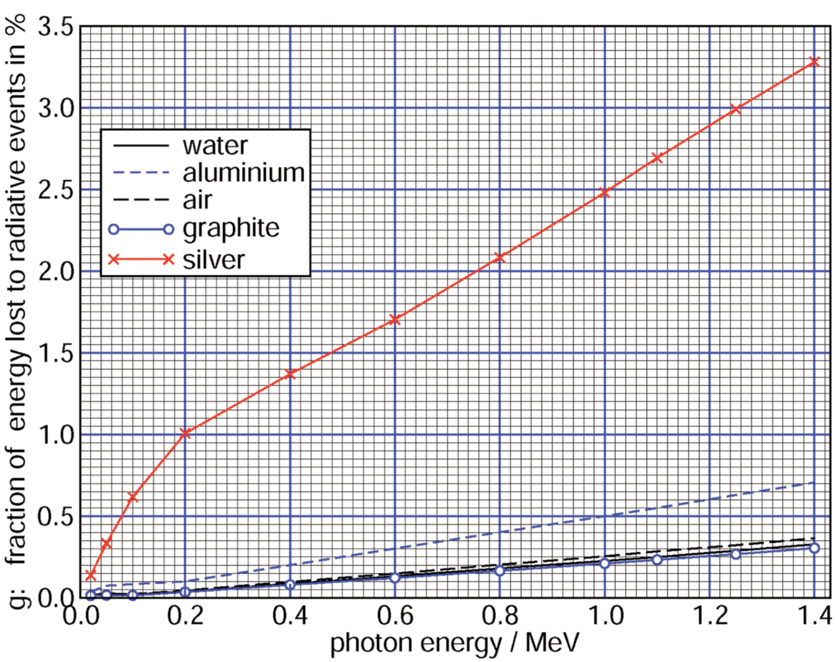

Figure A-23. $\overline{g}$ values for a variety of materials as a function of photon beam energy. Calculated using the EGSnrc user-code g with the XCOM datasets.

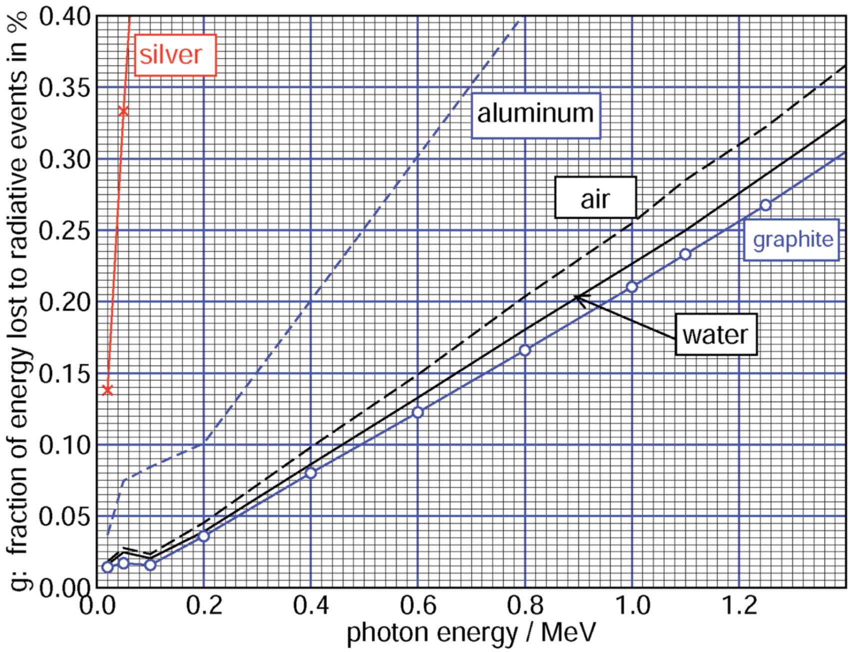

Figure A-24. As in figure A-23 with emphasis on low-*Z* materials.

6. Acknowledgments

I wish to thank Chris Soares, John Schreiner, and Tim Olding for help getting the compositions of the radiochromic film and gel dosimeter materials and Steve Seltzer for providing the ESTAR program many years ago.

References

Attix, F. H. *Introduction to Radiological Physics and Radiation Dosimetry.* New York: Wiley Interscience, 1986.

Berger, M. J. (1992). "ESTAR, PSTAR and ASTAR: Computer Programs for Calculating Stopping-Power and Ranges for Electrons, Protons, and Helium Ions. National Institute of Standards and Technology (NIST) Report NISTIR-4999 (Washington, DC). Available on-line at http://physics.nist.gov/Star.

Berger, M. J., and J. H. Hubbell. (1987). XCOM: Photon Cross Sections on a Personal Computer. Report NBSIR87–3597. Gaithersburg, MD: National Institute of Standards and Technology (NIST).

Burlin, T. E. "Cavity Chamber Theory" in *Radiation Dosimetry,* Vol I, Second edition. F. H. Attix and W. C. Roesch (eds.). New York: Academic Press, pp. 331–392, 1968.

Burlin, T. E. (1966). "A general theory of cavity ionization." *Br J Radiol* 39:727–734.

(ICRU) (1984). International Commission on Radiation Units and Measurements Report 37. Stopping Powers for Electrons and Positrons. Bethesda, MD: ICRU.

Kawrakow, I. (2000), "Accurate condensed history Monte Carlo simulation of electron transport. I. EGSnrc, the new EGS4 version." *Med Phys* 27:485–498.

Kawrakow, I. and D. W. O. Rogers. (2000). The EGSnrc Code System: Monte Carlo Simulation of Electron and Photon Transport, Technical Report PIRS–701. National Research Council of Canada, Ottawa, Canada.

Keall, P., and C. Baldock. (1999). "A theoretical study of the radiological properties and water equivalence of Fricke and polymer gels used for radiation dosiemtry." *Australas Phys Eng Sci Med* 22:85–91.

Seltzer, S. M. (1993). "Calculation of photon mass energy-transfer and mass energy-absorption coefficients (dosimetry application)." *Radiat Res* 136:147–170,

Zeng, G. G., M. R. McEwen, D. W. O. Rogers, and N. V. Klassen. (2005). "An experimental and Monte Carlo investigation of the energy dependence of alanine/EPR dosimetry: II. Clinical electron beams." *Phys Med Biol* 50:1119–1129.